



Trajectory tracking control of powered parafoil without velocity feedback

Panlong Tan · Zengqiang Chen · Qinglin Sun · Xiaoyu Zhang 

Received: 26 July 2022 / Accepted: 16 March 2023 / Published online: 20 June 2023
© The Author(s), under exclusive licence to Springer Nature B.V. 2023

Abstract High-precision trajectory tracking control of the powered parafoil (PPF) has been a challenging problem due to the nonlinear characteristics and multiple internal and external disturbances. Considering the nonlinearity and the cross-coupling dynamics between the control inputs of the PPF, the active disturbance compensation-based sliding mode control (SMC) strategy is proposed. The trajectory tracking control of the PPF is decomposed into lateral and longitudinal control channels, and the proposed controllers for each channel are designed separately. By applying the linear extended state observer (LESO), the nonlinear dynamics, cross-coupling effect and external wind disturbances are estimated and compensated as the total disturbance in each channel. To tackle the residual estimation error of the total disturbance, the SMC is applied. With the elaborately designed sliding manifold, the proposed method only requires the heading angle and altitude as feedbacks for the lateral and longitudinal control channels, respectively, while the angular velocity and horizontal velocity are not required. Specifically, both control channels are proved to be stable based on Lyapunov method. Simulation and semi-physical experimental results are provided to demonstrate the effectiveness of the proposed method

and superior control performance over other existing method.

Keywords Powered parafoil · Constraint analysis · Flexible-wing vehicle · Dynamic modeling · Sliding mode control · Active disturbance rejection control

1 Introduction

In recent years, the powered parafoil (PPF), as shown in Fig. 1, has been widely accepted for precise payload delivery and field investigation [1–6]. The steerable parafoil makes the PPF different from the traditional parachute systems. Due to the outstanding aerodynamic characteristics of the parafoil, the PPF is suitable for long distance delivery of heavy payloads with the advantages of high energy-efficiency, low costs, soft-landing capability, and inherent stability. The compact structure and foldable parafoil make the PPF easy to transport before the deployment. Moreover, the gliding characteristic of the parafoil ensures that the PPF has no risk for crash.

The PPF is composed of the parafoil and payload, and the payload is suspended strictly under the parafoil via suspension lines. Compared with the traditional parafoil airdrop systems [7–10], the PPF is more applicable with the altitude control capability. The control inputs for the PPF involve brake deflection and thrust, which are used to control lateral direction and longitudinal altitude, respectively. The asymmetric deflec-

P. Tan · Z. Chen · Q. Sun · X. Zhang (✉)
College of Artificial Intelligence, Nankai University,
Tianjin 300350, China
e-mail: zhangxiaoyu@nankai.edu.cn



Fig. 1 Powered parafoil

tion of the brake causes the yaw motion of the PPF, and the thrust effects the angle of attack of the parafoil and thus controls the altitude. Accordingly, the trajectory tracking problem can be decomposed into lateral and longitudinal control problems for simplicity. However, the PPF has strong nonlinearity and is susceptible to wind disturbances due to the low flight speed and lightweight parafoil [11]. Moreover, the payload of the PPF swings during the flight since it is suspended under the canopy. This structure makes PPF unable to use the real-time state information measured by high-precision inertial navigation system for control. The cross-coupling effect between the lateral and longitudinal control channels also makes the control problem more complicated. Therefore, the PPF has attracted considerable attention in academia, and many novel results about the application of the parafoil have been reported in the literature.

In the past decades, several control methods have been applied to the trajectory tracking of the PPF [12–15]. Garcia-Beltran [16] presented the development of passivity-based control (PBC) algorithms to stabilize an unmanned powered parachute aerial vehicle. Slegers [17] proposed a model predictive control (MPC) strategy for lateral heading control of the PPF, and a simplified linear dynamic model of six degrees of freedom (DOF) was applied as the predictive model. Ochi [18] and Li [19] employed a three-term PID controller, including the asymmetric brake deflection, symmetric brake, and thrust. These methods were developed and validated based on the linearized dynamic model, while

the nonlinear dynamics were not considered. By introducing the neural network to approximate the dynamic error, Liu [20] and Qian [21] proposed the nonlinear flight control methods for the lateral-directional relative yaw angle control and the trajectory tracking control of the PPF, respectively. In recent studies, the robust backstepping tracking control [22] and all-coefficient adaptive control (ACAC) [23] methods were also presented. Considering the complexity features of PPF, Xie [24,25] proposed an online subspace prediction method to overcome the uncertainties and disturbances and Sun [26] implemented the sliding mode control (SMC) to the PPF. Aoustin [27] designed a nonlinear control law for longitudinal motion control based on a new mathematical model, which was constructed as the system of two rigid bodies connected by an elastic joint with four DOF. However, most of the aforementioned methods depend on the linearized or precise models, which may reduce their robustness and lead weak capability to attenuate external disturbances. Moreover, it is easy to get accurate translational and angular velocity, while that is not available or expensive in practice.

Since the PPF is a complex nonlinear system and is susceptible to external wind disturbances, researchers turned to active disturbance rejection control (ADRC) methodology to enhance the robustness of the system [28–35]. The proposed method has demonstrated significant advantages in the control of nonlinear systems, including but not limited to aircraft control. Tao [36,37] applied the ADRC in the trajectory tracking control by regarding the uncertainties and external disturbances as the total disturbance which can be estimated and compensated actively. In the following studies, different conditions such as insufficient initial altitude [38] and various wind disturbances [39,40] are considered by Tao. Tan [41,42] designed the lateral and longitudinal controllers based on the ADRC separately and achieved satisfying performance based on simulations. Sun [43] proposed a hybrid control approach for PPF based on ADRC by considering that the wind interference and the unbalanced load on the actuators of its horizontal controller can extremely reduce the control effect. Luo proposed a lateral ADRC controller for the PPF based on the wind compensation to reduce the impact of the wind disturbance [44], and then the proposed method was applied to trajectory tracking control of the PPF based on wind identification [45]. The decoupling trajectory tracking control was also proposed to reduce the burden of ADRC by Luo [46,47]. However, when

the non-diminishing disturbances are introduced to the PPF, the estimation error of the total disturbance cannot be attenuated to zero, resulting in the limitation of the controller to achieve better performance. The asymptotic stability of the PPF was also not guaranteed.

In this paper, only GPS is selected to acquire the position of the PPF for cost saving, and the sliding mode control [48–51], which has shown strong robustness to the nonlinear systems, is introduced to handle the residual estimation error of the total disturbance of LESO, and a novel control scheme is proposed to ensure the asymptotic stability of the PPF. Considering the practice that the altitude and direction are the only states that can be controlled, the trajectory tracking problem is decomposed into the lateral and longitudinal control channels and the tracking controllers for each channel are designed. The 3D trajectory can be decomposed into horizontal and height targets according to the characteristics of PPF. With the elaborately designed sliding manifold, the proposed method guarantees the asymptotic stability of the desired equilibrium point even in the presence of unknown non-diminishing disturbances. The asymptotic stability of the PPF is proved by rigorous mathematical analysis based on Lyapunov method. Specifically, the heading angles for the lateral channel and the altitude for the longitudinal channel are the only required state feedback, which can enhance the robustness of the proposed method. That is, the PPF can be stabilized to the desired trajectory without velocity feedback. Moreover, the proposed method is validated by simulations and semi-physical experiments.

The remaining parts of the paper are organized as follows. Section 2 presents the eight DOF dynamic model of the PPF. Then, a complete analysis for the proposed method is provided in Sect. 3. In Sects. 4 and 5, simulation and experimental results are provided to evaluate the performance of PPF, respectively. The concluding remarks are presented in Sect. 6.

2 Modeling of the powered parafoil

A practical PPF is shown in Fig. 1. Due to the aerodynamic characteristics of parafoil and the non-rigid internal connections, the PPF has complex dynamic characteristics. Therefore, the modeling problem of the PPF is addressed firstly in this section.

Considering the relative motion between the canopy and payload, a model with eight DOF is proposed. Fig-

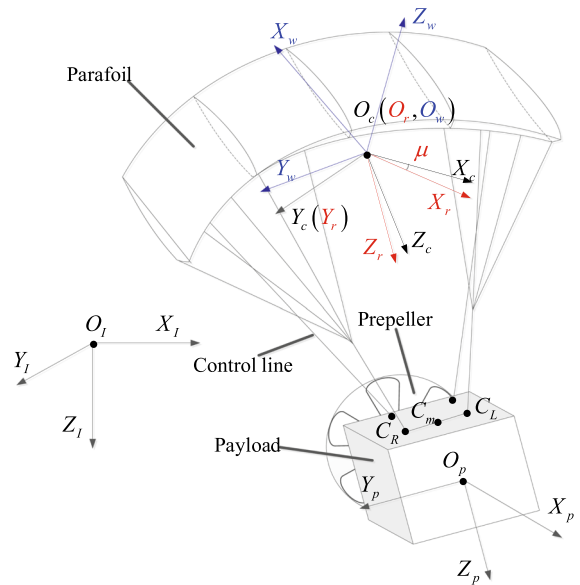


Fig. 2 Coordinate systems

ure 2 shows the configuration of the PPF and three main coordinate systems are presented, including geodetic coordinate system (inertial coordinate system) Σ_I , parafoil-fixed coordinate system Σ_c and payload-fixed coordinate system Σ_p . These coordinate systems are fixed to a fixed point at the ground, the center of gravity (CG) of the parafoil and the CG of the payload, respectively. Specifically, to facilitate the lift and drag calculation of the parafoil, the rigging coordinate system Σ_r and wind coordinate system Σ_w are established as auxiliary coordinate systems. In Fig. 2, $O, X, Y,$ and Z are origin, x-axis, y-axis and z-axis of the corresponding coordination, respectively, and the sub-script represents the corresponding coordination. C_R, C_L and C_m are the right suspension point, the left suspension point, and the center of the two suspension points, respectively. Note that all the coordinate systems are right-handed.

By using the Lagrange approach, the basic equations of motion for the payload in Σ_p are given by

$$\frac{\partial \mathbf{P}_p}{\partial t} + \omega_p \times \mathbf{M}_p = \mathbf{F}_p^a + \mathbf{F}_p^G + \mathbf{F}_p^{th} + \mathbf{F}_p^{te} \tag{1}$$

$$\frac{\partial \mathbf{H}_p}{\partial t} + \mathbf{V}_p \times \mathbf{P}_p + \omega_p \times \mathbf{H}_p = \mathbf{M}_p^{te}$$

where $\mathbf{P}_p, \mathbf{H}_p, \mathbf{F}_p^G, \mathbf{F}_p^a, \mathbf{F}_p^{te}$ and $\mathbf{F}_p^{th} \in \mathbf{R}^{3 \times 1}$ are momentum, moment of momentum, gravity, aerodynamic force, tension of suspension line and the thrust provided by the propeller, respectively. $\mathbf{M}_p^{te} \in \mathbf{R}^{3 \times 1}$

is the moment of the tension of suspension lines. The payload is assumed to be in a regular shape and the moments of the gravity, thrust and aerodynamic drag are neglected. The forces acting on the payload are described in Σ_p with the subscript p . The superscripts a, G, te and th indicate different type of forces, respectively. $\mathbf{V}_p = [u_p \ v_p \ w_p]^T$ and $\omega_p = [p_p \ q_p \ r_p]^T$ are the velocity and angular rate of the payload, and the superscript T here is the transpose symbol.

The basic equations of motion for the parafoil in Σ_c are

$$\frac{\partial \mathbf{P}_c}{\partial t} + \omega_c \times \mathbf{P}_c = \mathbf{F}_c^a + \mathbf{F}_c^G + \mathbf{F}_c^{te} \tag{2}$$

$$\frac{\partial \mathbf{H}_c}{\partial t} + \mathbf{V}_c \times \mathbf{P}_c + \omega_c \times \mathbf{H}_c = \mathbf{M}_c^a + \mathbf{M}_c^{te}$$

where $\mathbf{P}_c, \mathbf{H}_c, \mathbf{F}_c^G, \mathbf{F}_c^a$ and \mathbf{F}_c^{te} are momentum, moment of momentum, gravity, aerodynamic force and tension of suspension lines, which are represented in Σ_c , respectively. $\mathbf{M}_c^{te} \in \mathbf{R}^{3 \times 1}$ is moment of the tension of suspension lines in Σ_c and $\mathbf{M}_c^a \in \mathbf{R}^{3 \times 1}$ is the moment caused by aerodynamic force. $\mathbf{V}_c = [u_c \ v_c \ w_c]^T$ and $\omega_c = [p_c \ q_c \ r_c]^T$ denote the velocity and angular rate of the parafoil, where the subscript c denotes the parafoil-fixed coordinate system Σ_c .

Applying the velocity and force constraints between the parafoil and payload, the dynamic model of the PPF can be proposed. Let $\dot{x} = [\dot{V}_p \ \dot{\omega}_p \ \dot{V}_c \ \dot{\omega}_c \ \mathbf{F}_c^{te} \ m_x^{te} \ m_z^{te}]^T$ be the time derivative of the state vectors, then 17 equations are obtained. Hereto, the motion of equations of the PPF is described as

$$\dot{x} = M^{-1}F \tag{3}$$

where M and F derived from the dynamic and constraint equations. Specifically, the $\mathbf{F}_c^{te}, m_x^{te}$ and m_z^{te} are calculated as auxiliary states, which are useful in mechanical analysis. The detailed descriptions of the proposed model refer to Ref. [52].

3 Problem formulation and main results

The control inputs for the PPF involve lateral brake deflection of the canopy trailing edge and thrust provided by the propeller, which are utilized to control lateral direction and altitude of the PPF, respectively. The main objective of this paper is to maintain trajectory tracking control of the PPF. To this end, the control laws of two inputs are designed.

3.1 Problem formulation

According to the structure of the PPF, the trajectory tracking problem of the PPF can be solved by designing the lateral and longitudinal control channels. Let ψ_l and h , respectively, be the lateral direction angle and longitudinal altitude, then the lateral and longitudinal control channels can be described as

$$\begin{cases} \ddot{\psi}_l = b_\psi(x) \delta_a + f_\psi(x) \\ \ddot{h} = b_h(x) F_{th} + f_h(x) \end{cases} \tag{4}$$

where $b_\psi(x), b_h(x), f_\psi(x)$ and $f_h(x)$ are lateral control gain, longitudinal control gain, lateral nonlinear dynamics and longitudinal nonlinear dynamics, respectively. $\delta_a = \delta_R - \delta_L$ is the asymmetric deflection and δ_R and δ_L are the deflection control of the right and left trailing edge, respectively. F_{th} denotes the first term of \mathbf{F}_p^{th} . Then the control objective is decomposed into tracking the desired altitude h_d and tracking the reference heading angle ψ_d . According to the practical constraints of the PPF, the horizontal tracking errors can only be eliminated by control the course of the PPF. Therefore, the reference of the lateral control channel is designed as $\psi_d = \psi_r + \text{atan}(e_p/k_e)$, where ψ_r is the heading angle of the reference trajectory, e_p is the horizontal position error, and k_e is a positive constant.

3.2 Controller design

To facilitate the analysis, the lateral and longitudinal control channels are designed to share the control schemes. The model of both channels can be simplified as

$$\begin{cases} \dot{\xi}_1 = \xi_2 \\ \dot{\xi}_2 = b_\xi u + f_\xi \end{cases} \tag{5}$$

where $\xi_1 = \psi_l, \xi_2 = \dot{\psi}_l, b_\xi = b_\psi, f_\xi = f_\psi$ and $u = \delta_a$ for the lateral channel and $\xi_1 = h, \xi_2 = \dot{h}, b_\xi = b_h, f_\xi = f_h$ and $u = F_{th}$ for the longitudinal channel. In order to estimate the total disturbance of each channel with LESO, the system Eq. (5) can be augmented as

$$\begin{cases} \dot{\xi}_1 = \xi_2 \\ \dot{\xi}_2 = b_0 u + \xi_3 \\ \dot{\xi}_3 = w \end{cases} \tag{6}$$

where $\xi_3 = f_\xi + (b_\xi - b_0)$ is the augmented state, which is called the total disturbance, and w is the

derivative of total disturbance. Then, the LESO can be designed as

$$\begin{cases} \dot{z}_1 = z_2 + \beta_1 \varepsilon_1 \\ \dot{z}_2 = b_0 u + z_3 + \beta_2 \varepsilon_1 \\ \dot{z}_3 = \beta_3 \varepsilon_1 \end{cases} \quad (7)$$

where $\varepsilon_1 = \xi_1 - z_1$ is the estimation error and z_i ($i = 1, 2, 3$) is the estimated value of ξ_i ($i = 1, 2, 3$). The estimation error of LESO can be expressed as

$$\begin{cases} \dot{\varepsilon}_1 = \varepsilon_2 - 3\varepsilon_1 \\ \dot{\varepsilon}_2 = \varepsilon_3 - 3\varepsilon_1 \\ \dot{\varepsilon}_3 = w - \varepsilon_1 \end{cases} \quad (8)$$

where $\varepsilon_2 = \xi_2 - z_2$ and $\varepsilon_3 = \xi_3 - z_3$. In particular, the observer gains can be selected as

$$[\beta_1, \beta_2, \beta_3]^T = [3\omega_o, 3\omega_o^2, \omega_o^3]^T \quad (9)$$

with $\omega_o > 0$ for simplicity. If ξ_1 (i.e., ψ_l or h) is the only feedback state and to achieve the trajectory tracking of the PPF via SMC methodology, the sliding manifold can be elaborately designed as

$$\sigma = c_0 e_1 + \varepsilon_2 + \int_0^t k_s \operatorname{sgn}(e_1) ds \quad (10)$$

where $e_1 = \xi - \xi_d$ and $\varepsilon_2 = z_2 - \dot{\xi}_d$. ξ_d is the reference second order differentiable and $\dot{\xi}_d$ is the derivative of ξ_d , respectively. $\operatorname{sgn}(z)$ denotes the standard sign function, which is defined as

$$\operatorname{sgn}(z) = \begin{cases} 1, & z > 0 \\ 0, & z = 0 \\ -1, & z < 0 \end{cases} \quad (11)$$

To ensure that ε_1 converges to zero asymptotically, the control law of system (5) can be designed as

$$u = \frac{1}{b_0} (-c_0 \varepsilon_2 - k_1 \sigma - k_2 \operatorname{sgn}(\sigma) - k_s \operatorname{sgn}(e_1) - z_3 - \beta_2 \varepsilon_1) \quad (12)$$

where c_0, k_1, k_2, k_s are positive parameters.

3.3 Stability analysis

Due to practical constraints, the PPF works in a domain of interest of $D = \{\xi \mid \|\xi\| \leq \delta\}$, where $\xi = [\xi_1, \xi_2]^T$ and δ is positive constant. The stability of the proposed control strategy will be analyzed within D . Before proceeding with the subsequent analysis, the following assumption is made.

Assumption 1 The derivative of ξ_3 is bounded within D and

$$|w| \leq L_w \quad (13)$$

where L_w is a positive constant.

To facilitate the subsequent stability analysis, a compact set B_ε is defined as

$$B_\varepsilon = \{\varepsilon \mid \|\varepsilon\| \leq \delta_\varepsilon\}$$

where $\varepsilon = [\varepsilon_1 \ \varepsilon_2 \ \varepsilon_3]^T$ and δ_ε is a positive constant. The LESO states are initialized to ensure that $\|\varepsilon(0)\|$ is within B_ε .

Theorem 1 The estimation error of the observer presented in Eq. (8) is bounded and

$$\lim_{\omega_o \rightarrow \infty, t \rightarrow \infty} \|\varepsilon\| = 0. \quad (14)$$

Proof Let $\eta_i = \frac{\varepsilon_i}{\omega_o^i}$ ($i = 1, 2, 3$), then Eq. (8) can be rewritten as

$$\begin{cases} \dot{\eta}_1 = \eta_2 - \beta_1 \eta_1 \\ \dot{\eta}_2 = \eta_3 - \beta_2 \eta_1 \\ \dot{\eta}_3 = \frac{w}{\omega_o^3} - \beta_3 \eta_1 \end{cases} \quad (15)$$

And Eq. (15) can be reformulated as

$$\dot{\eta} = A_\eta \eta + B_\eta \frac{w}{\omega_o^3} \quad (16)$$

for simplicity, where $\eta = [\eta_1, \eta_2, \eta_3]^T$ and

$$A_\eta = \begin{bmatrix} -3 & 1 & 0 \\ -3 & 0 & 1 \\ -1 & 0 & 0 \end{bmatrix}, B_\eta = \begin{bmatrix} 0 \\ 0 \\ 1 \end{bmatrix} \quad (17)$$

It is clear that A_η is Hurwitz. Then, there exists a unique positive definite matrix P_η which satisfies a Lyapunov equation $A_\eta^T P_\eta + P_\eta A_\eta = -Q_\eta$. By choosing the Lyapunov function candidate as $V(\eta) = \eta^T P_\eta \eta$, the derivative of $V(\eta)$ can be written as

$$\begin{aligned} \dot{V}(\eta) &= -\omega_o \eta^T Q_\eta \eta + 2\eta^T P_\eta B_\eta \frac{w}{\omega_o^3} \\ &\leq -\omega_o \lambda_{\min}(Q_\eta) \|\eta\|^2 + \frac{2L_w \lambda_{\max}(P_\eta) \|\eta\|}{\omega_o^3} \end{aligned} \quad (18)$$

Considering $\frac{V(\eta)}{\lambda_{\max}(P_\eta)} \leq \|\eta\|^2 \leq \frac{V(\eta)}{\lambda_{\min}(P_\eta)}$, inequality (18) can be rearranged as

$$\begin{aligned} \dot{V}(\eta) \leq & -\frac{\omega_o \lambda_{\min}(Q_\eta)}{\lambda_{\max}(P_\eta)} V(\eta) \\ & + \frac{2L_w \lambda_{\max}(P_\eta)}{\omega_o^3 \sqrt{\lambda_{\min}(P_\eta)}} \sqrt{V(\eta)} \end{aligned} \tag{19}$$

Let $W = \sqrt{V(\eta)}$, then $\dot{W} = \frac{V(\eta)}{2\sqrt{V(\eta)}}$ can be derived. Inequality (19) can be rewritten as

$$\dot{W} \leq -\frac{\omega_o \lambda_{\min}(Q_\eta)}{2\lambda_{\max}(P_\eta)} W + \frac{2L_w \lambda_{\max}(P_\eta)}{\omega_o^3 \sqrt{\lambda_{\min}(P_\eta)}} \tag{20}$$

Applying the Gronwall–Bellman inequality, one obtains

$$\begin{aligned} W \leq & -\left(\frac{2L_w \lambda_{\max}^2(P_\eta)}{\omega_o^4 \sqrt{\lambda_{\min}(P_\eta)} \lambda_{\min}(Q_\eta)} - W(t_0) \right) \\ & e^{-\frac{\lambda_{\min}(Q_\eta)}{2\lambda_{\max}(P_\eta)}(t-t_0)} + \frac{2L_w \lambda_{\max}^2(P_\eta)}{\omega_o^4 \sqrt{\lambda_{\min}(P_\eta)} \lambda_{\min}(Q_\eta)} \end{aligned} \tag{21}$$

which indicates that when $t \rightarrow \infty$, one gets

$$\begin{aligned} \|\eta\| \leq & \frac{\sqrt{V}}{\sqrt{\lambda_{\min}(P_\eta)}} \\ \leq & \frac{2L_w \lambda_{\max}^2(P_\eta)}{\omega_o^4 \lambda_{\min}(P_\eta) \lambda_{\min}(Q_\eta)} \\ = & \frac{M_e}{\omega_o^4} \end{aligned} \tag{22}$$

Since P_η and Q_η are independent from ω_o , Eq. (22) indicates that

$$\lim_{\omega_o \rightarrow \infty, t \rightarrow \infty} \|\eta\| = 0 \tag{23}$$

which together with $\eta_i = \frac{e_i}{\omega_o^i}$ ($i = 1, 2, 3$) yields

$$\lim_{\omega_o \rightarrow \infty, t \rightarrow \infty} \|\varepsilon\| \leq \lim_{\omega_o \rightarrow \infty, t \rightarrow \infty} \omega_o^3 \|\eta\| = 0 \tag{24}$$

Furthermore, if ω_o is tuned to ensure that $\frac{M_e}{\omega_o} \leq \delta_\varepsilon$, the estimation error of the LESO can always be limited within the compact set B_ε . This completes the proof. \square

Theorem 2 *Regarding the system (5), the proposed control law (12) guarantees that the tracking error converges to zero asymptotically.*

Proof For clarity, the proof of Theorem 2 is completed within two steps. It is first demonstrated that the designed control law can drive the error state to the desired manifold. And then, the convergence of the error state is proved.

Step 1: To analysis the convergence of σ , a Lyapunov function candidate can be designed as $V_1 = \frac{1}{2}\sigma^2$. Then, by substituting the proposed control law (12), the time derivative of V_1 can be written as

$$\begin{aligned} \dot{V}_1 &= \sigma \dot{\sigma} \\ &= \sigma (c_0 e_2 + b_0 u + z_3 + \beta_2 \varepsilon_1 + k_s \operatorname{sgn}(e_1)) \\ &= \sigma (c_0 \varepsilon_2 + c_0 \varepsilon_2 + b_0 u + z_3 + \beta_2 \varepsilon_1 + k_s \operatorname{sgn}(e_1)) \\ &= \sigma (-k_1 \sigma - k_2 \operatorname{sgn}(\sigma) + c_0 \varepsilon_2) \\ &= -k_1 \sigma^2 - k_2 |\sigma| + \sigma c_0 \varepsilon_2 \end{aligned} \tag{25}$$

With $k_2 \geq c_0 \delta_\varepsilon$, Eq. (25) can be rewritten as

$$\begin{aligned} \dot{V}_1 &\leq -k_1 \sigma^2 - k_2 |\sigma| + \sigma c_0 \varepsilon_2 \\ &\leq -(k_2 - c_0 \delta_\varepsilon) |\sigma| \\ &= -k_\sigma |\sigma| \\ &= -k_\sigma V_1^{\frac{1}{2}} \\ &\leq 0 \end{aligned} \tag{26}$$

where $k_\sigma = (k_2 - c_0 \delta_\varepsilon)$ is a positive constant. Equation (26) indicates that σ is asymptotically convergent. Moreover, Eq. (26) also shows that σ converges to zero in finite time.

Step 2: When the sliding manifold is reached and $\sigma = 0$ is maintained, it can be inferred from Eq. (10) that

$$e_2 = \dot{e}_2 + \varepsilon_2 = -c_0 e_1 - \int_0^t k_s \operatorname{sgn}(e_1) ds + \varepsilon_2 \tag{27}$$

where e_2 is the derivative of e_1 . Substituting Eq. (27) into the equation of $\dot{e}_1 = e_2$, one gets

$$\dot{e}_1 = -c_0 e_1 - \int_0^t k_s \operatorname{sgn}(e_1) ds + \varepsilon_2 \tag{28}$$

and it can be reorganized as

$$\begin{cases} \dot{e}_1 = -c_0 e_1 + z_\gamma \\ \dot{z}_\gamma = -k_s \operatorname{sgn}(e_1) + \dot{\varepsilon}_2 \\ = -k_s \operatorname{sgn}(e_1) + \varepsilon_3 - \beta_2 \varepsilon_2 \end{cases} \tag{29}$$

To proceed the analysis, the Lyapunov function candidate can be designed as

$$V_2 = \frac{1}{2} (c_0 e_1 - z_\gamma)^2 + (1 + \alpha) \int_0^{e_1} h(s) ds + \alpha \frac{1}{2} z_\gamma^2 \tag{30}$$

where α is a positive constant and $h(e_1) = k_s \operatorname{sgn}(e_1) - \varepsilon_3 + \beta_2 \varepsilon_2$. Note that $e_1 h(e_1) \geq 0$ is ensured with

Table 1 Characteristic parameters of the PPF

| Symbol | Description | Value |
|-----------|------------------------|----------------------|
| b | Wing span | 11.18/m |
| \bar{c} | Mean aerodynamic chord | 2.23/m |
| t | Thickness | 0.34/m |
| μ | Rigging angle | -7° |
| S_c | Wing area | 24.97/m ² |
| l_c | O_c to O_m | 6.28/m |
| l_p | O_m to O_p | 0.5/m |
| l | O_m to $O_R(O_L)$ | 0.25/m |
| m_c | Mass of parafoil | 6.9/kg |
| m_p | Mass of payload | 76.5/kg |
| S_p | Payload area | 0.6/m ² |

$k_s \geq (1 + \beta_2) \delta_\epsilon$. Then, V_2 is positive definite. Differentiating V_2 gets

$$\dot{V}_2 = (c_0 e_1 - z_\gamma) (c_0 \dot{e}_1 - \dot{z}_\gamma) + (1 + \alpha) h(e_1) \dot{e}_1 + \alpha z_\gamma \dot{z}_\gamma = -c_0 (c_0 e_1 - z_\gamma)^2 - \alpha e_1 h(e_1) \leq 0. \tag{31}$$

Therefore, it is proved in Eq. (31) that e_1 converges to zero asymptotically. Moreover, further analysis yields that $e_2 = 0$ when e_1 is kept at zero. The proof is completed. \square

4 Simulations analysis

To evaluate the performance of the proposed method, numerical simulation analysis is presented in this section. The dynamic model of the PPF is formulated as aforementioned in Sect. 2, and the physical characteristics of a certain type of the PPF are listed in Table 1.

The proposed dynamic model of the PPF is validated by experiment, and the analysis is presented in [52]. The control parameters of the proposed controller are listed in Table 2.

As a comparison, the conventional LADRC is applied in the analysis. The control law is given by

$$u = \frac{k_p e_1 + k_d e_2 - z_3}{b_0} \tag{32}$$

and the control parameters of the two control channels are shown in Table 3. Note that the control parameters of the conventional LADRC are quite different with the equivalent parameters of the proposed method. It is tested that the conventional LADRC controller with similar parameters as the proposed method revealed unstable control performance.

Table 2 Control parameters of the proposed controller

| Control channel | c_0 | k_1 | k_2 | k_s | b_0 | ω_o |
|-----------------|-------|-------|-------|-------|-------|------------|
| Lateral | 1.9 | 0.1 | 0.05 | 0.02 | 0.8 | 10 |
| Longitudinal | 0.05 | 0.45 | 0.1 | 0.1 | 0.12 | 20 |

Table 3 Control parameters of the comparative controller

| Control channel | k_p | k_d | b_0 | ω_o |
|-----------------|-------|-------|-------|------------|
| Lateral | 0.19 | 2 | 0.8 | 10 |
| Longitudinal | 0.022 | 0.5 | 0.12 | 20 |

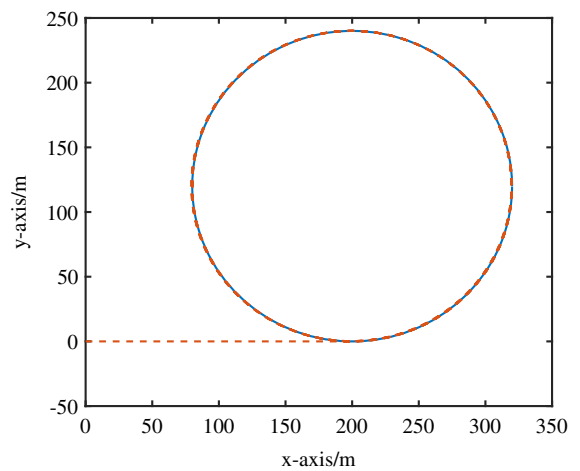


Fig. 3 Circular trajectory—trajectories in the horizontal plane (solid line: reference, dashed line: the proposed method, dotted line: LADRC)

4.1 Circular trajectory

The PPF is controlled to track a circular trajectory with a fixed altitude in this case. The reference trajectory is a circle with a radius of 120 m and the reference altitude is 160 m. In the simulation settings, the initial velocities are set as $V_c = V_p = [8 \ 0 \ 1.5]^T$ m/s and the initial position of the CG of Σ_c is set as $L_p = [0 \ 0 \ 230]^T$ m. The other states are set to be zero for simplicity. Considering that the wind has severe impact on the control performance of the PPF, the wind $V_w = [1 \ 2 \ 0]$ m/s is added to the simulation at 200 s to evaluate the robustness of the controllers. The simulation time is set as 400 s, and the results are shown in Figs. 3, 4, 5, 6. Note that the control inputs are zero in the first 20 s to make sure that the PPF has maintained steady state.

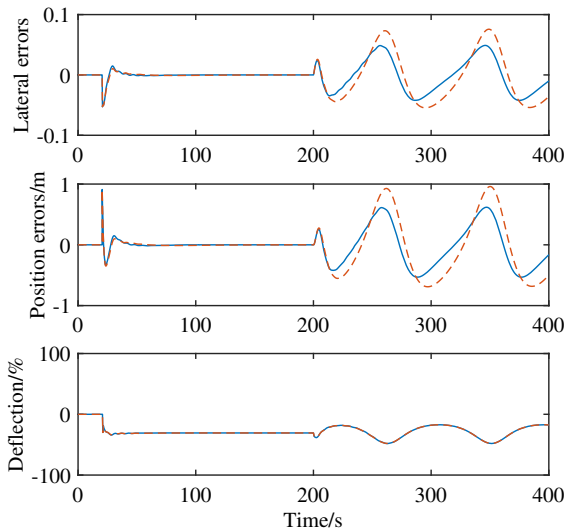


Fig. 4 Circular trajectory—lateral tracking errors and deflections (solid line: the proposed method, dashed line: LADRC)

The controlled horizontal trajectories of the PPF are shown in Fig. 3. And Fig. 4 shows the horizontal tracking errors and the corresponding control inputs. It can be seen that both the proposed and the comparative controllers can achieve the control objective with the position errors less than 1 m. The performance of the proposed controller is similar with the LADRC during the first 200 s. When the wind disturbance is added to simulation at 200 s, Fig. 4 shows that the maximum horizontal position error of the proposed controller in wind environment is 0.65 m and that of the LADRC controller is 0.97 m, which indicates that the proposed method can achieve better performance than the LADRC. According to Fig. 5, the PPF is stabilized at the reference altitude under the control of both proposed and LADRC controllers. The simulation results in the first figure of Fig. 5 indicate that the proposed controller can maintain the altitude of 160 m with a settling time of 76.32 s, while that of the LADRC is 89.47 s. When the wind is added to the simulation, both controllers can compensate the disturbance actively and keep the altitude unaffected. Therefore, the control performance of the proposed method is validated.

4.2 S-path trajectory

To facilitate mathematical description, the reference trajectory of the PPF is usually composed of lines and arcs. In this case, the trajectory tracking simulation of the S-path with three line segments is provided. With

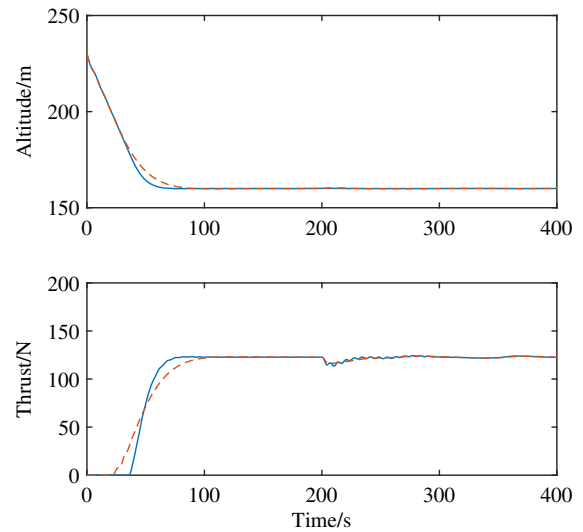


Fig. 5 Circular trajectory—altitude and thrust (solid line: reference, dashed line: the proposed method, dotted line: LADRC)

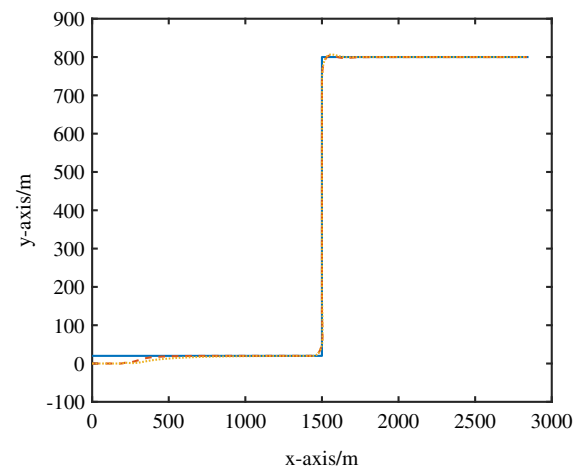


Fig. 6 S-path trajectory—trajectories in the horizontal plane (solid line: reference, dashed line: the proposed method, dotted line: LADRC)

the aim to evaluate the performance of controllers under strict conditions, the line segments in S-path are connected directly and the arcs are not used. The simulation settings are the same with circular trajectory except the wind. After completing the simulation, the results are recorded in Figs. 6, 7 and 8.

The reference and controlled horizontal trajectories are shown in Fig. 6, and the comparative results of the lateral channel are illustrated in Fig. 7. Unlike the quadrotors, the PPF cannot track the trajectories with sharp corners due to the limited control inputs. There-

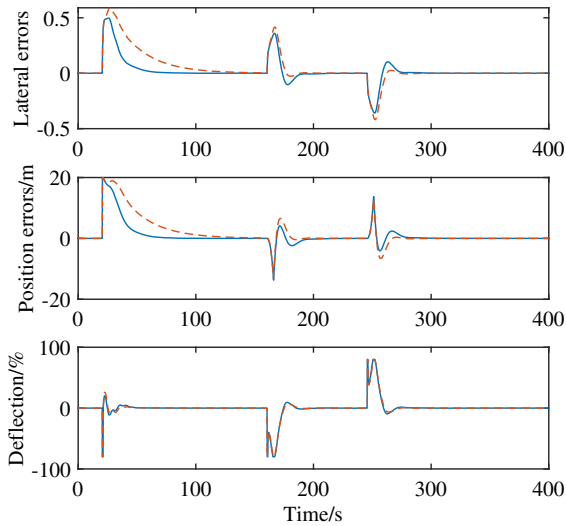


Fig. 7 S-path trajectory—lateral tracking errors and deflections (solid line: the proposed method, dashed line: LADRC)

fore, as shown in the subplot 2 of Fig. 7, the lateral position errors occur at every corner of the reference. It is also seen that the lateral position errors can converge to zero. Comparing the proposed controller and LADRC, it can be seen that the position errors of the proposed controller is stabilized to zero from 20 m with a settling time of 54.38 s, while that of the LADRC is 84.56 s. The comparison of Fig. 7 indicates that the proposed method is superior to LADRC in the lateral channel. In the longitudinal channel, the altitude is well controlled even at the reference corners. The thrust output of both the proposed and comparative controllers yields oscillations due to the coupling effect between the lateral and longitudinal control channels when the reference is changed to another line segment at corners. Figure 8 indicates that both controllers show good control effect in steady state, while the proposed controller achieves better transient performance than the comparative one with less settling time. More precisely, the settling time of the proposed method is 79.45 s, while that of the LADRC is 91.27 s.

4.3 Robustness verification

The robustness is an important objective of controller development. In order to verify the robustness of the PPF with the proposed controller, the Monte-Carlo simulation technique is applied in this paper. Considering the practice that the PPF is applied to take various

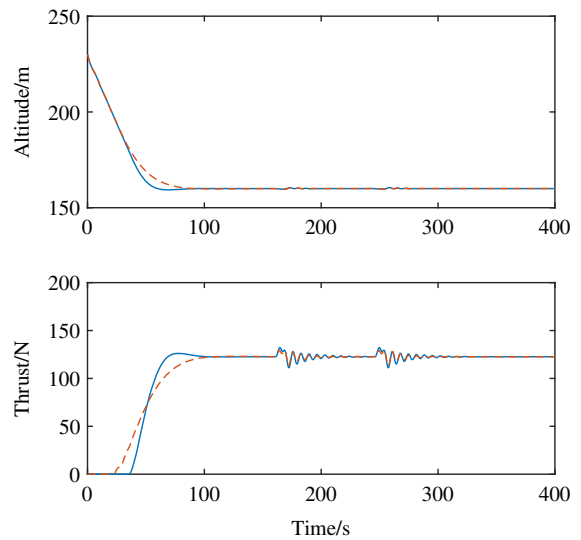


Fig. 8 S-path trajectory—altitude and thrust (solid line: reference, dashed line: the proposed method, dotted line: LADRC)

loads, the mass of the payload is set to vary uniformly with $\pm 30\%$. The MC simulation results with 50 sets of stochastic payloads are investigated and the results are shown in Figs. 9 and 10. The circular reference is applied, and the wind is also added as external disturbances. It can be found in the figures that the lateral position errors and longitudinal altitude errors are influenced by the changing of payload. Compared with Fig. 4, Fig. 10 shows that the maximum lateral position error is expanded from 1 m to 6 m. It is also seen that the settling time of the longitudinal channel is varied from 73.52 to 82.39 s with the payload. However, all the simulation results show that the lateral and longitudinal tracking errors are driven to zero by the proposed controller. Then, the robustness of the proposed method is verified by the Monte-Carlo simulations.

5 Semi-physical experimental analysis

5.1 Experimental setup

Due to the GPS positioning accuracy and measurement noise, the trajectory tracking performance of the PPF will be influenced in practical applications. To further investigate the effectiveness of the proposed method, the semi-physical platform with the self-designed flight controller unit and the proposed dynamic model is designed and the experiment is performed on it. The dynamic model is applied to simulate the PPF and to

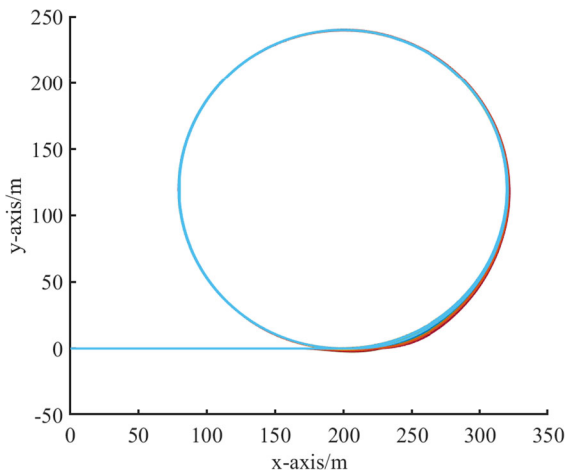


Fig. 9 Monte-Carlo test—trajectories in the horizontal plane

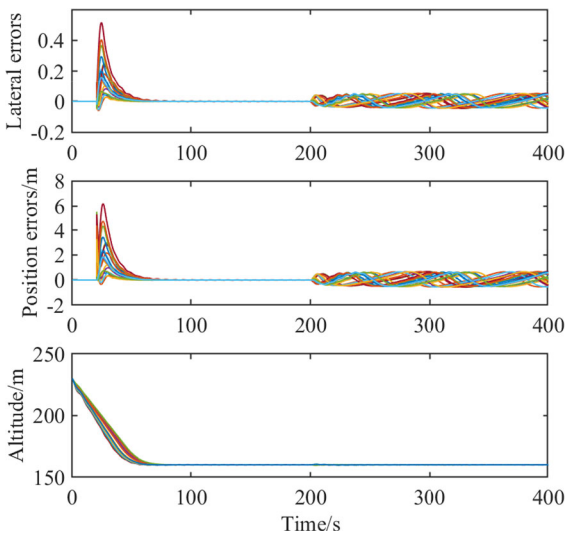


Fig. 10 Monte-Carlo test—lateral and longitudinal tracking errors

generate the GPS data encoded by GPGGA format. In the flight controller unit, the ARM microprocessors STM32F407 and STM32F103 are used as the main and auxiliary processor, respectively. The proposed method is programmed and implemented in the main processor, and the rudders and the thrust motor are controlled by the auxiliary processor for safety. This structure ensures the computing capacity as well as reliability of the PPF. Figure 11 shows the control system of the PPF. The positions and heading angles are measured with a sample frequency of 1 Hz from the dynamic model and transmitted to the flight controller via serial port. Then,

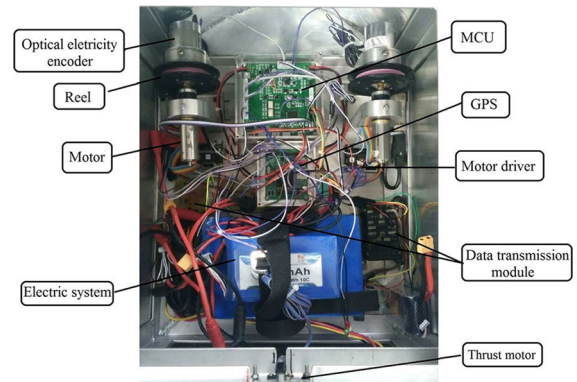


Fig. 11 Rudders and flight controller unit

the control inputs are calculated in the main processor and send to the dynamic model.

5.2 Experimental results

The initial conditions of this experiment are configured as the simulation of the circular trajectory, and the corresponding experimental results are recorded in Figs. 12, 14. Figures 12 and 13 show that the proposed method and LADRC can attenuate the lateral position errors and maintain the trajectory tracking objective. Compared with Fig. 4, it is seen from the subplot 2 of Fig. 13 that lateral position errors of the proposed method and LADRC are larger than that of the simulation due to the discretization of the controller. It also can be found that the proposed method can achieve faster convergence of the lateral errors than LADRC before the wind is added. During 200–400 s, it is shown in Fig. 13 that the proposed method can achieve smaller lateral position errors than the LADRC. The same conclusion can be drawn from the comparison in Fig. 14. Specifically, it can be found that the proposed method has a overshoot of 5.62 m and a settling time of 154.33 s, which are much lower than that of the LADRC. The experiment and comparative analyses show that the proposed method can achieve better transient and stable performance than LADRC in wind environment.

6 Conclusion

In this paper, a novel SMC method for the PPF was proposed based on the disturbance compensation. By deriving the dynamic model of the PPF, the trajectory tracking problem was decomposed into the lateral and

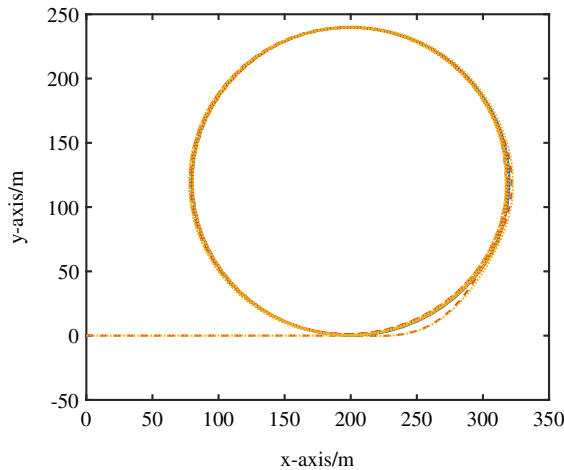


Fig. 12 Experiment—trajectories in the horizontal plane (solid line: reference, dashed line: the proposed method, dotted line: LADRC)

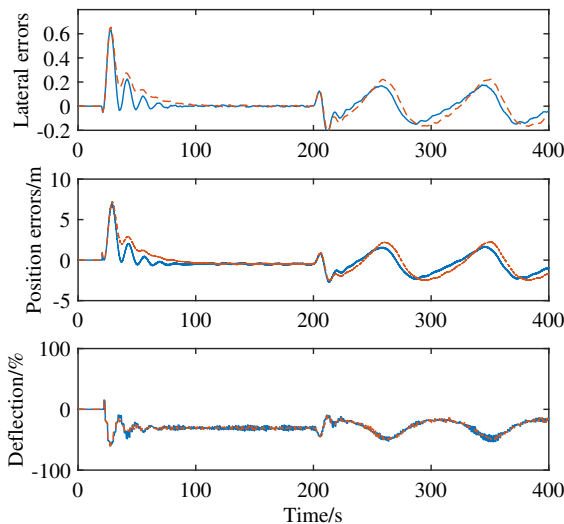


Fig. 13 Experiment—lateral tracking errors and deflections (solid line: the proposed method, dashed line: LADRC)

longitudinal control channels. The nonlinear dynamics of each channel and the coupling effect between the two channels were considered as the total disturbances, which were estimated and compensated actively. With the elaborately designed sliding manifold, the proposed control law ensured the asymptotic convergence of the PPF. Specifically, the heading angle and the altitude were the only required feedback states in the proposed control scheme. The closed-loop stability of the PPF was proved by rigorous mathematical analysis based on Lyapunov techniques. Finally, the numerical simulations of different reference trajectories, Monte-Carlo

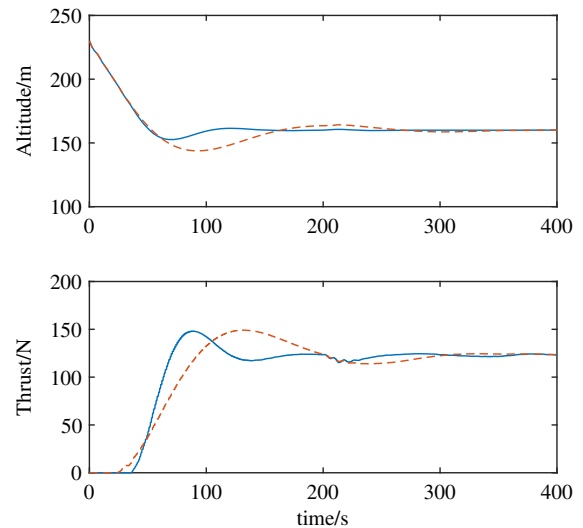


Fig. 14 Experiment—altitude and thrust (solid line: reference, dashed line: the proposed method, dotted line: LADRC)

test, and experiment were performed to evaluate the performance of the proposed method. Through comparative analysis, it is shown that the proposed method achieved better tracking performance than the LADRC. In the future, we will seek to implement the proposed method to the practical PPF platform with better control performance. In the meanwhile, wind resistance and steerability performance need to be further studied.

Funding This work was supported by the National Natural Science Foundation of China (Grant Nos. 62103204, 61973172 and 61973175) and the keyTechnologies Research and Development Program of Tianjin (Grant No. 19JCZDJC32800).

Data Availability Enquiries about data availability should be directed to the authors.

Declarations

Conflict of interest The authors declare that they have no conflict of interest.

Human and animal rights This article does not contain any studies with human participants or animals performed by any of the authors.

References

1. Lee, S.J., Arena Jr. A.S.: Autonomous parafoil return-to-point vehicle for high altitude ballooning. In: AIAA Guidance, Navigation, and Control Conference 2014 - SciTech Forum and Exposition 2014, January 13, 2014 - January 17, 2014, AIAA Guidance, Navigation, and Control Conference (2014)

2. Slegers, N., Brown, A., Rogers, J.: Experimental investigation of stochastic parafoil guidance using a graphics processing unit. *Control. Eng. Pract.* **36**, 27–38 (2015)
3. Tan, P., Sun, Q., Chen, Z., Jiang, Y.: Characteristic model based generalized predictive control and its application to the parafoil and payload system. *Optim. Control Appl. Methods* **40**(4), 659–675 (2019)
4. Sun, H., Sun, Q., Luo, S., Chen, Z., Wannan, W., Tao, J., He, Y.: In-flight compound homing methodology of parafoil delivery systems under multiple constraints. *Aerosp. Sci. Technol.* **79**, 85–104 (2018)
5. Sun, H., Luo, S., Sun, Q., Chen, Z., Wannan, W., Tao, J.: Trajectory optimization for parafoil delivery system considering complicated dynamic constraints in high-order model. *Aerosp. Sci. Technol.* **98**, 105631 (2020)
6. Sun, H., Wang, F., Sun, Q., Chen, Z., Tao, J.: Distributed consensus algorithm for multiple parafoils in mass airdrop mission based on disturbance rejection. *Aerosp. Sci. Technol.* **109**, 1–12 (2021)
7. Sun, H., Luo, S., Sun, Q., Chen, Z., Wannan, W., Tao, J.: Trajectory optimization for parafoil delivery system considering complicated dynamic constraints in high-order model. *Aerosp. Sci. Technol.* **98**, 1–13 (2020)
8. Dek, C., Overkamp, J.L., Toeter, A., Hoppenbrouwer, T., Slimmens, J., van Zijl, J., Naeije, M.: A recovery system for the key components of the first stage of a heavy launch vehicle. *Aerosp. Sci. Technol.* **100**, 1–9 (2020)
9. Li, B., He, Y., Han, J., Xiao, J.: A new modeling scheme for powered parafoil unmanned aerial vehicle platforms: theory and experiments - sciencedirect. *Chin. J. Aeronaut.* **32**(11), 2466–2479 (2019)
10. Zhu, E., Sun, Q., Tan, P., Chen, Z., Kang, X., He, Y.: Modeling of powered parafoil based on kirchhoff motion equation. *Nonlinear Dyn.* **79**(1), 617–629 (2014)
11. Zhu, H., Sun, Q., Liu, X., Liu, J., Chen, Z.: Fluid structure interaction based aerodynamic modeling for flight dynamics simulation of parafoil system. *Nonlinear Dyn.* **104**(6), 1–22 (2021)
12. Devalla, V., Mondal, A.K., Prakash, A.A.J., Prateek, M., Prakash, O.: Guidance, navigation and control of a powered parafoil aerial vehicle. *Curr. Sci.* **111**(6), 1045–1054 (2016)
13. Devalla, V., Om, P.: Longitudinal and directional control modeling for a small powered parafoil aerial vehicle. In: AIAA Atmospheric Flight Mechanics Conference, AIAA AVIATION Forum. American Institute of Aeronautics and Astronautics (2016)
14. Cacan, M.R., Scheuermann, E., Ward, M.B., Costello, M., Reinert, C., Shurtliff, M.: Shared control of a guided parafoil and payload system. In: 23rd AIAA Aerodynamic Decelerator Systems Technology Conference, Aerodynamic Decelerator Systems Technology Conferences. American Institute of Aeronautics and Astronautics (2015)
15. Cacan, M.R., Ward, M.B., Scheuermann, E., Costello, M.: Human-in-the-loop control of guided airdrop systems. In: AIAA Guidance, Navigation, and Control Conference, AIAA SciTech Forum. American Institute of Aeronautics and Astronautics (2015)
16. Garcia-Beltran, C.D., Miranda-Araujo, E.M., Guerrero-Sanchez, M.E., Valencia-Palomo, G., Hernandez-Gonzalez, O., Gomez-Penate, S.: Passivity-based control laws for an unmanned powered parachute aircraft. *Asian J. Control* **23**(5), 2087–2096 (2021)
17. Slegers, N., Costello, M.: Model predictive control of a parafoil and payload system. In: Collection of Technical Papers - AIAA Atmospheric Flight Mechanics Conference, August 16, 2004 - August 19, 2004, volume 1 of Collection of Technical Papers - AIAA Atmospheric Flight Mechanics Conference, pp. 67–86. American Institute of Aeronautics and Astronautics Inc. (2004)
18. Ochi, Y., Kondo, H., Watanabe, M.: Linear dynamics and pid flight control of a powered paraglider. In: AIAA Guidance, Navigation, and Control Conference, Guidance, Navigation, and Control and Co-located Conferences. American Institute of Aeronautics and Astronautics (2009)
19. Li, B., Yang, L., He, Y., Han, J.: Energy-based controller decoupling of powered parafoil unmanned aerial vehicle. In: 2016 IEEE International Conference on Cyber Technology in Automation, Control and Intelligent Systems (CYBER), 19–22 June 2016, 2016 IEEE International Conference on Cyber Technology in Automation, Control and Intelligent Systems (CYBER), pages 313–20. IEEE (2016)
20. Liu, L., Yan, J.: Powered parafoil lateral-directional attitude angle control with adaptive neural network. In: 2010 Asia-Pacific International Symposium on Aerospace Technology, APISAT 2010, September 13, 2010–September 15, 2010, Proceedings of 2010 Asia-Pacific International Symposium on Aerospace Technology, APISAT 2010, pp. 714–718. Northwestern Polytechnical University (2010)
21. Qian, K., Chen, Z.: Dynamic inversion based on neural network applied to nonlinear flight control system. In: Proceedings of the 2010 2nd International Conference on Future Computer and Communication, ICFCC 2010, volume 1 of *Proceedings of the 2010 2nd International Conference on Future Computer and Communication, ICFCC 2010*, pp. V1699–V1703. IEEE Computer Society (2010)
22. Chen, Z., Zhang, H., Wei, J., Lijun, S., Qiu, J.: Robust backstepping tracking control based on nonlinear disturbance observer for unmanned parafoil vehicle. *Control Decis.* **32**(8), 1427–33 (2017)
23. Tan, P., Sun, Q., Jiang, Y., Zhu, E., Chen, Z., He, Y.: Trajectory tracking of powered parafoil based on characteristic model based all-coefficient adaptive control. *J. Central South Univ.* **24**(5), 1073–1081 (2017)
24. Xie, Z., Chen, Z., He, Y.: Online subspace predictive control of unmanned powered parafoil. *Inf. Control* **40**(6), 841–5 (2011)
25. Xie, Z., Chen, Z., Lv, J.: Sdre and series approximations model predictive control for a parafoil system. In: 2011 International Conference on Electric Information and Control Engineering, ICEICE 2011 - Proceedings, 2011 International Conference on Electric Information and Control Engineering, ICEICE 2011 - Proceedings, pp. 2562–2565. IEEE Computer Society (2011)
26. Sun, Q., Li, Yu., Zheng, Y., Tao, J., Sun, H., Sun, M., Dehmer, M., Zengqiang, C.: Trajectory tracking control of powered parafoil system based on sliding mode control in a complex environment. *Aerosp. Sci. Technol.* **122**, 1–10 (2022)
27. Aoustin, Y., Martynenko, Y.: Control algorithms of the longitude motion of the powered paraglider. In: Proceedings of the Asme 11th Biennial Conference on Engineering Systems Design and Analysis, 2012, Vol 1, Proceedings of the Asme

- 11th Biennial Conference on Engineering Systems Design and Analysis, 2012, Vol 1, pp. 775–784, New York, 2012. Amer Soc Mechanical Engineers
28. Jing Qing Han: From PID to active disturbance rejection control. *IEEE Trans. Industr. Electron.* **56**(3), 900–906 (2009)
 29. Cai, R., Zhou, H., Chunhai, K.: Boundary disturbance rejection for fractional distributed parameter systems via the sliding mode and riesz basis approach. *Nonlinear Dyn.* **111**(2), 1355–1367 (2022)
 30. Godbole, A.R., Subbarao, K.: Nonlinear control of unmanned aerial vehicles with, cable suspended payloads. *Aerosp. Sci. Technol.* **93**, 1–11 (2019)
 31. Sun, L., Jin, Y., You, F.: Active disturbance rejection temperature control of open-cathode proton exchange membrane fuel cell. *Appl. Energy* **261**, 1–13 (2020)
 32. Song, M., Panfeng, H.: Dynamics and anti-disturbance control for tethered aircraft system. *Nonlinear Dyn.* **110**(3), 2383–2399 (2022)
 33. Carlos, A.I., Hebertt, S.R., Miguel, S.C.: A linear active disturbance rejection control for a ball and rigid triangle system. *Mathematical Problems in Engineering*, 2016:1–11 (2016)
 34. Michalek, M.M., Lakomy, K., Adamski, W.: Robust output-feedback cascaded tracking controller for spatial motion of anisotropically-actuated vehicles. *Aerosp. Sci. Technol.* **92**, 915–929 (2019)
 35. Zhang, Z., Zhao, T.: Based on robust sliding mode and linear active disturbance rejection control for attitude of quadrotor load uav. *Nonlinear Dyn.* **108**(4), 3485–3503 (2022)
 36. Tao, J., Sun, Q., Tan, P., Chen, Z., He, Y.: Active disturbance rejection control (adrc)-based autonomous homing control of powered parafoils. *Nonlinear Dyn.* **86**(3), 1461–1476 (2016)
 37. Tao, J., Sun, Q., Chen, Z., He, Y.: Autonomous homing control of a parafoil system based on ADRC. In: 7th IEEE Chinese Guidance, Navigation and Control Conference, CGNCC 2016, August 12, 2016 - August 14, 2016, CGNCC 2016–2016 IEEE Chinese Guidance, Navigation and Control Conference, pp. 110–115. Institute of Electrical and Electronics Engineers Inc. (2016)
 38. Tao, J., Sun, Q., Tan, P., Chen, Z., He, Y.: Autonomous homing control of a powered parafoil with insufficient altitude. *ISA Trans.* **65**, 516–524 (2016)
 39. Tao, J., Qing, L.S., Wei, L., Zeng, Q.C.: CFD based dynamic modelling of parafoil systems in the wind environment. In: Uncertainty Modelling in Knowledge Engineering and Decision Making - 12th International Fuzzy Logic and Intelligent Technologies in Nuclear Science Conference. FLINS 2016, August 24, 2016–August 26, 2016, Uncertainty Modelling in Knowledge Engineering and Decision Making - Proceedings of the 12th International FLINS Conference, FLINS 2016, pp. 668–674. World Scientific Publishing Co., Pte Ltd (2016)
 40. Tao, J., Sun, Q., Sun, H., Chen, Z., Dehmer, M., Sun, M.: Dynamic modeling and trajectory tracking control of parafoil system in wind environments. *IEEE/ASME Trans. Mechatron.* **22**(6), 2736–2745 (2017)
 41. Tan, P., Sun, Q., Zhu, E., Chen, Z.: Active disturbance rejection control design for trajectory tracking of parafoil and payload system. *J. Comput. (Taiwan)* **27**(2), 59–66 (2016)
 42. Tan, P., Sun, Q., Chen, Z.: Application of active disturbance rejection control in trajectory tracking of powered parafoil system. *J. Zhejiang Univ. (Eng. Sci.)* **51**(5), 992–999 (2016)
 43. Sun, H., Sun, Q., Tao, J., Luo, S., Chen, Z.: A hybrid control approach for powered parafoil combining active disturbance rejection control and unbalanced load compensation. *Proc. Inst. Mech. Eng. Part IJ. Syst. Control Eng.* **232**(3), 299–314 (2018)
 44. Luo, S., Sun, Q., Sun, M., Sun, H., Wu, W., Chen, Z.: Lateral control approach of powered parafoils combining wind feedforward compensation with active disturbance rejection control. In: 14th IEEE/ASME International Conference on Mechatronic and Embedded Systems and Applications, MESA 2018, July 2, 2018–July 4, 2018, 14th IEEE/ASME International Conference on Mechatronic and Embedded Systems and Applications, MESA 2018. Institute of Electrical and Electronics Engineers Inc. (2018)
 45. Luo, S., Tan, P., Sun, Q., Wannan, W., Luo, H., Chen, Z.: In-flight wind identification and soft landing control for autonomous unmanned powered parafoils. *Int. J. Syst. Sci.* **49**(5), 929–946 (2018)
 46. Luo, S., Sun, Q., Sun, M., Tan, P., Wannan, W., Sun, H., Chen, Z.: On decoupling trajectory tracking control of unmanned powered parafoil using adrc-based coupling analysis and dynamic feedforward compensation. *Nonlinear Dyn.* **92**(4), 1619–1635 (2018)
 47. Luo, S., Sun, Q., Wannan, W., Sun, M., Chen, Z., He, Y.: Accurate flight path tracking control for powered parafoil aerial vehicle using adrc-based wind feedforward compensation. *Aerosp. Sci. Technol.* **84**, 904–915 (2019)
 48. Xing, L., Zhang, J., Liu, C., Zhang, X.: Fuzzy-logic-based adaptive event-triggered sliding mode control for spacecraft attitude tracking. *Aerospace science and technology*, **108** (2021)
 49. Cao, G., Liu, Y., Jiang, Y., Zhang, F., Bian, G., Owens, D.H.: A novel sliding surface design for predefined-time stabilization of Euler-Lagrange systems. *Nonlinear Dyn.* **105**(1), 371–386 (2021)
 50. Li, B., Zhang, H., Xiao, B., Wang, C., Yang, Y.: Fixed-time integral sliding mode control of a high-order nonlinear system. *Nonlinear Dyn.* **107**(1), 909–920 (2022)
 51. Trentin, J.F.S., Santos, D.A.: Predefined-time global sliding mode control design for a 3D pendulum. *Nonlinear Dyn.* **109**(3), 1693–1704 (2022)
 52. Tan, P., Sun, M., Sun, Q., Chen, Z.: Dynamic modeling and experimental verification of powered parafoil with two suspending points. *IEEE Access* **8**, 12955–12966 (2020)

Publisher's Note Springer Nature remains neutral with regard to jurisdictional claims in published maps and institutional affiliations.

Springer Nature or its licensor (e.g. a society or other partner) holds exclusive rights to this article under a publishing agreement with the author(s) or other rightsholder(s); author self-archiving of the accepted manuscript version of this article is solely governed by the terms of such publishing agreement and applicable law.